



# Periods and Frequency Drifts of Groups of the Decimetric Spikes in Two Solar Flares

Marian Karlický<sup>1</sup> · Jaroslav Dudík<sup>1</sup> · Ján Rybák<sup>2</sup>

Received: 10 June 2024 / Accepted: 5 August 2024 / Published online: 21 August 2024  
© The Author(s) 2024

## Abstract

We studied the radio emission occurring as narrowband decimetric spikes observed during the 10 May 2022 and 26 August 2022 flares. In the radio spectra, these spikes were distributed in groups that occurred quasi-periodically with the periods 5.1 s in the 10 May 2022 flare and 9.1 s in the 26 August 2022 flare. In some parts of these groups, even subgroups of spikes distributed with the quasi-periods of 0.19 s (10 May 2022 flare), and 0.17 s and 0.21 s (26 August 2022 flare) were found. Some of these subgroups even drifted to higher or lower frequencies, which was observed for the first time. At the time of the dm-spikes observation, a pair of reconnecting loops are identified in the SDO/AIA EUV observations of the 10 May 2022 flare, one of which is interpreted as belonging to a small erupting filament. We propose that these loops reconnect in the dynamic quasi-periodic regime (the period 0.19 s) and this reconnection is modulated by an oscillation of one of the interacting loops (the period 5.1 s). Accelerated electrons from this process are trapped in reconnecting plasma outflows, and thus the drifting groups of spikes are generated. The 26 August 2022 flare is a complex event with several systems of bright loops; nevertheless, it also shows a disintegrating erupting filament similar to the 10 May 2022 flare, meaning that the dm-spikes are likely generated by similar reconnection processes.

**Keywords** Flares · Dynamics · Radio bursts · Dynamic spectrum

## 1. Introduction

The decimetric spikes belong to the most interesting solar radio bursts, because they seem to be connected with the primary flare process (Droege 1977; Staehli and Magun 1986; Guedel 1990; Krucker and Benz 1994; Aschwanden, Dennis, and Benz 1998; Bouratzis et al. 2016; Karlický et al. 2022). Their brightness temperature is up to  $10^{15}$  K. In the radio spectrum, they occur in clouds of many narrowband bursts with a relative bandwidth of about 1–3% and duration less than 100 ms (Benz 1986).

Many models of the dm-spikes were proposed. Among them, the most probable models are based on the electron-cyclotron maser mechanism (ECM) (Melrose and Dulk 1982;

---

✉ J. Rybák  
rybak@astro.sk

<sup>1</sup> Astronomical Institute, Czech Academy of Sciences, 251 65 Ondřejov, Czech Republic

<sup>2</sup> Astronomical Institute, Slovak Academy of Sciences, 059 60 Tatranská Lomnica, Slovakia

Winglee, Dulk, and Pritchett 1988; Fleishman and Mel'nikov 1998; Fleishman, Gary, and Nita 2003; Melrose 2017) or on the plasma emission mechanism: a) with the upper-hybrid waves (Stepanov et al. 1999; Bárta and Karlický 2001) or b) with the Bernstein modes (Willes and Robinson 1996; Karlický, Benáček, and Rybák 2021). Whereas in ECM models, it is assumed that the ratio  $Y = \omega_{pe}/\omega_{ce} \leq 1$ , where  $\omega_{pe}$  and  $\omega_{ce}$  are the electron plasma and electron cyclotron frequencies, and the electromagnetic emission (spikes) is generated directly, in the plasma emission models with  $Y > 1$ , the electromagnetic emission is produced by a two-step process (first some electrostatic waves and then conversion into electromagnetic waves).

As known, the parameters of the dm-spikes depend on frequency. For example, the spike half-maximum duration  $\tau$  depends on the frequency  $f$  as  $\tau \sim f^{-1.29}$  (Rozhansky, Fleishman, and Huang 2008). Furthermore, distributions of spike bandwidths in dependence on frequency have the power-law form (Nita et al. 2014). Tan (2013) analyzed the small-scale microwave bursts (SMBs) in long-duration flares. He has shown that their brightness temperatures are  $8.18 \times 10^{11} - 1.92 \times 10^{13}$  K, lifetimes are 5–18 ms, relative frequency bandwidths are 0.7–3.5%, and they have superhigh frequency drifting rates. Karlický, Sobotka, and Jiříčka (1996) and Karlický, Benáček, and Rybák (2021) studied the frequency bandwidths of spikes by the Fourier method. They found the power-law spectra with power-law indices close to  $-5/3$ . Similar results were found by Messmer and Benz (2000). Because the power-law indices are close to the Kolmogorov turbulence index  $-5/3$ , it was suggested that the narrowband dm-spikes are generated by superthermal electrons in the magnetohydrodynamic (MHD) turbulence in the magnetic reconnection outflows (Karlický, Sobotka, and Jiříčka 1996; Karlický, Benáček, and Rybák 2021).

In this paper, we present and analyze periods and frequency drifts of groups of the dm-spikes. According to our knowledge, the frequency drift of spike groups is presented for the first time. Using SDO/AIA images, we tried to identify the location of spike sources. In the 10 May 2022 flare, interacting loops were recognized at times of dm-spikes. Therefore we interpret the period and frequency drifts of the groups of spikes in a model of magnetic reconnection between these loops. In the 26 August 2022 flare, many overlapping systems of loops were seen in channels of AIA, showing a rather complicated magnetic structure. Therefore it was impossible to recognize the reconnecting structure connected with the dm-spikes. Nevertheless, we think that the spikes observed in this flare were generated by similar processes as in the 10 May 2022 flare.

## 2. Observations of dm-Spikes and Their Analysis

We use radio data from the Ondřejov radiospectrograph operating in the 800–2000 MHz frequency range with the spectral and time resolutions 4.7 MHz and 0.01 s, respectively (Jiříčka and Karlický 2008). As known, the calibration of the solar radio spectrometers is complicated problem; see, e.g., Tan et al. (2015). Our radio spectral data are calibrated only in the relation to the radio flux recorded before the flare. For this reason, we present the radio flux in arbitrary units (a.u.).

### 2.1. Event 1 – X1.5 Flare on 10 May 2022

On 10 May 2022, during a preflare activity of the X1.5-class flare (start 13:50, maximum 13:55, and end 13:59 UT; see Section 3.1) in the time interval 13:41:40–13:42:20 UT and in the 1000–1400 MHz frequency range, groups of the dm-spikes were observed (see the

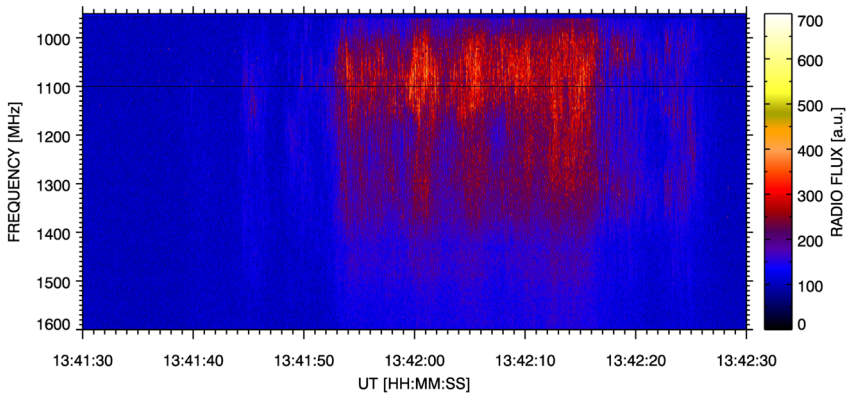


**Figure 1** Radio spectrum in the 900–1600 MHz range at 13:41:30–13:42:30 UT observed during the 10 May 2022 flare. The black line at 1100 MHz marks the frequency for which the wavelet analysis was made; see Figure 5.

**Table 1** Periods and frequency drifts detected in groups of the dm-spikes. Series duration corresponds to that of spike groups shown in Figures 1–4. For frequency drifts, see examples in these figures marked by the white lines.

Series duration (s)	Time (UT)	Frequency (MHz)	Periods (s)	Frequency drifts (MHz s <sup>-1</sup> )
Event: 10 May 2022				
60	13:41:30–13:42:30	1100	5.1	-
3	13:42:00–13:42:03	1140	0.19	~ +1100
Event: 26 August 2022				
60	06:23:00–06:24:00	1100	9.1	-
2	06:23:06–06:23:08	1040	0.21	~ -1000 ~ +1710
1	06:23:27–06:23:28	1150	0.17	~ -1330 ~ +930

900–1600 MHz radio spectrum in Figure 1 and Table 1). Typical lifetimes and relative frequency bandwidths of the spikes are ~ 10–20 ms and 0.7–1.5%, respectively. As seen in Figure 1, the spike groups appear quasi-periodically. A detailed view of these spikes in the 13:42:00–13:42:03 UT time interval is shown in Figure 2. Here, in the 1000–1400 MHz range, spikes drift to higher frequencies with the frequency drift of about 1100 MHz s<sup>-1</sup> (Table 1).

### 2.2. Event 2 – C7.2 Flare on 26 August 2022

On 26 August 2022, during a C7.2-class flare (start 06:07, maximum 06:28, and end 06:45 UT; see Section 3.2) in the time interval 06:23:10–06:23:45 UT and in the 800–1400 MHz range, the second case of the quasi-periodic groups of spikes was observed (see the 800–1500 MHz radio spectrum in Figure 3 and Table 1). Typical lifetimes and relative frequency bandwidths of the spikes are ~ 10–30 ms and 0.7–1.4%, respectively. Details of these spikes in two intervals (06:23:06–06:23:08 UT and 06:23:27–06:23:28 UT) are

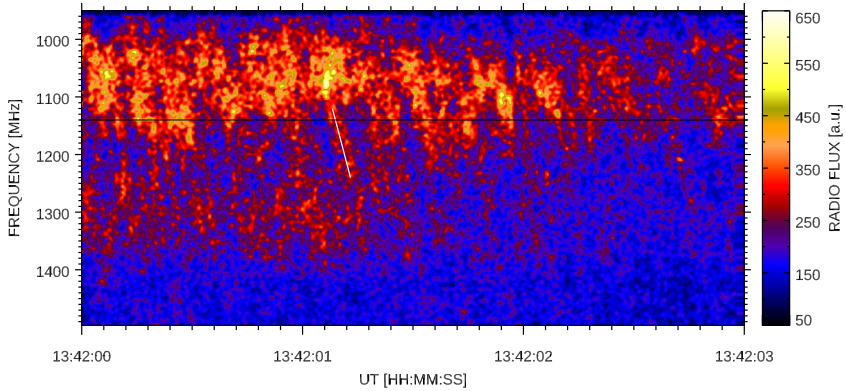


**Figure 2** Detailed radio spectrum in the 900–1500 MHz range at 13:42:00–13:42:03 UT observed during the 10 May 2022 flare. The black line at 1140 MHz shows the frequency for which the wavelet analysis was made; see Figure 6. The white line marks an example of the frequency drift of these spikes.

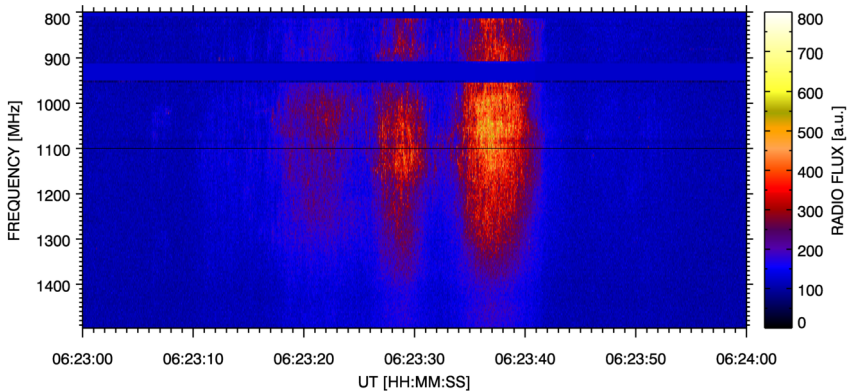


**Figure 3** Radio spectrum in the 800–1500 MHz range and the 06:23:00–06:24:00 UT time interval observed during the 26 August 2022 flare. The black line at 1100 MHz marks the frequency for which the wavelet analysis was made; see Figure 7.

shown in Figure 4 (upper and bottom panels). In both spectra, the positive and negative frequency drifts can be seen. For values of these frequency drifts, see Table 1.

### 2.3. Wavelet Analysis

Our analysis searched for quasi-periodic variations of radio flux in the radio spectra of the spike groups. We used the wavelet transform (WT) as it is described by Torrence and Compo (1998) deriving clear detection of the time–frequency evolution of the strong radio wave patterns. The Morlet mother wavelet, consisting of a complex sine wave modulated by a Gaussian, was used to search for radio signal variability with the nondimensional frequency  $\omega_0$  with padding the data. For our analysis, the value of the significance level was set to 95%. Both the calculated significance of the derived WT periodicities and the cone-of-influence were considered.

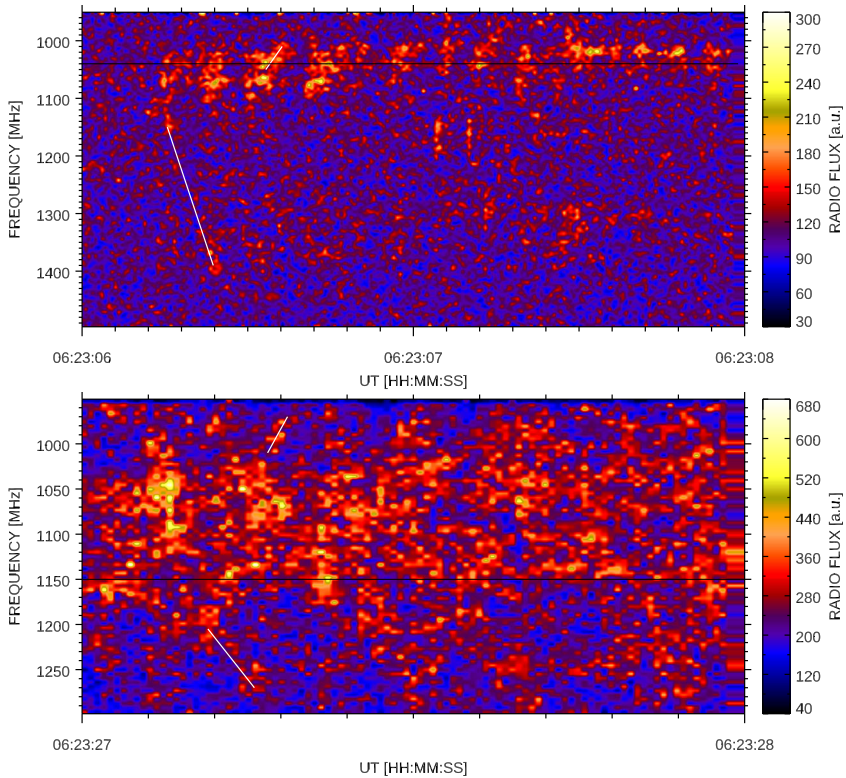


**Figure 4** Detailed radio spectra in the 950–1500 MHz range at 06:23:06–06:23:08 UT (upper panel) and in the 950–1300 MHz range at 06:23:27–06:23:28 UT (bottom panel) observed during the 26 August 2022 flare. The black lines at 1040 MHz in the upper panel and 1150 MHz in the bottom panel show the frequencies for which the wavelet analysis was made; see Figures 8 and 9. The white lines show examples of the frequency drifts of these spikes.

For all presented radio spectra, in their time and frequency intervals, we selected some single-frequency records and computed the corresponding wavelet power and integrated spectra; see Figures 5 and 6 for Event 1 and Figures 7, 8, and 9 for Event 2. Figure 5 presents the radio flux at 1100 MHz in the 13:41:30–13:42:30 UT time interval for the 10 May 2022 event. The wavelet power and integrated spectra show the significant period 5.1 s for the time interval 13:41:50–13:42:28 UT. For the same event, Figure 6 shows the radio flux at 1140 MHz and the wavelet power and integrated spectra in the 13:42:00–13:42:03 UT time interval. In this case, the period 0.19 s was found to be present in the time interval 13:42:00.15–13:42:02.10 UT.

Furthermore, Figures 7–9 show examples for the 26 August 2022 event: a) In Figure 7 the radio flux at 1100 MHz, its wavelet power, and integrated spectra in the 06:23:00–06:24:00 UT time interval. Here the period is 9.1 s significant for the time interval 06:23:14–06:23:45 UT; b) In Figure 8 the radio flux at 1040 MHz, its wavelet power, and integrated spectra in the 06:23:06–06:23:08 UT time interval. Here the period is 0.21 s significant for the time interval 06:23:06.3–06:23:07.4 UT; c) In Figure 9 the radio flux at 1150 MHz, its wavelet power, and integrated spectra in the 06:23:27–06:23:28 UT time

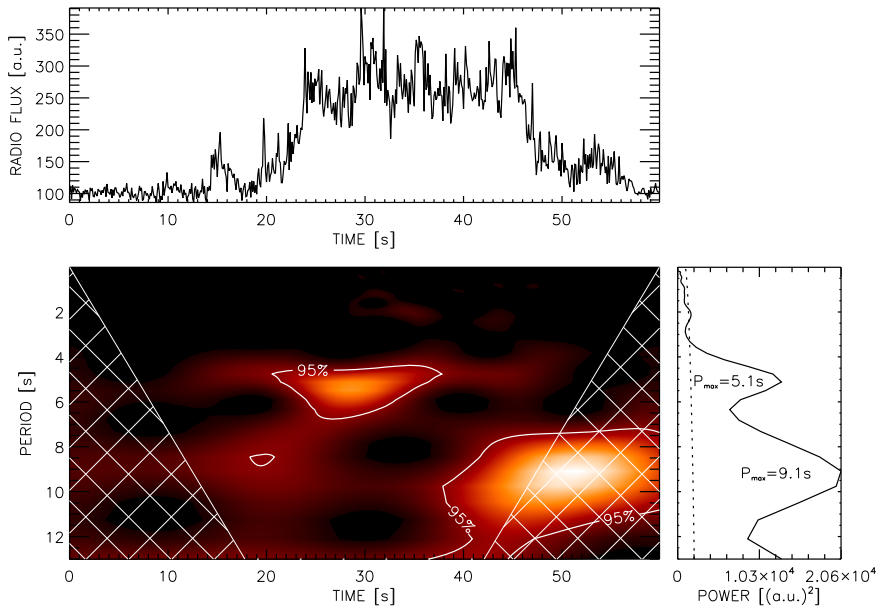


**Figure 5** The 1100 MHz radio flux, its wavelet power spectrum, and integrated spectrum in the 13:41:30 – 13:42:30 UT time interval of the 10 May 2022 event.

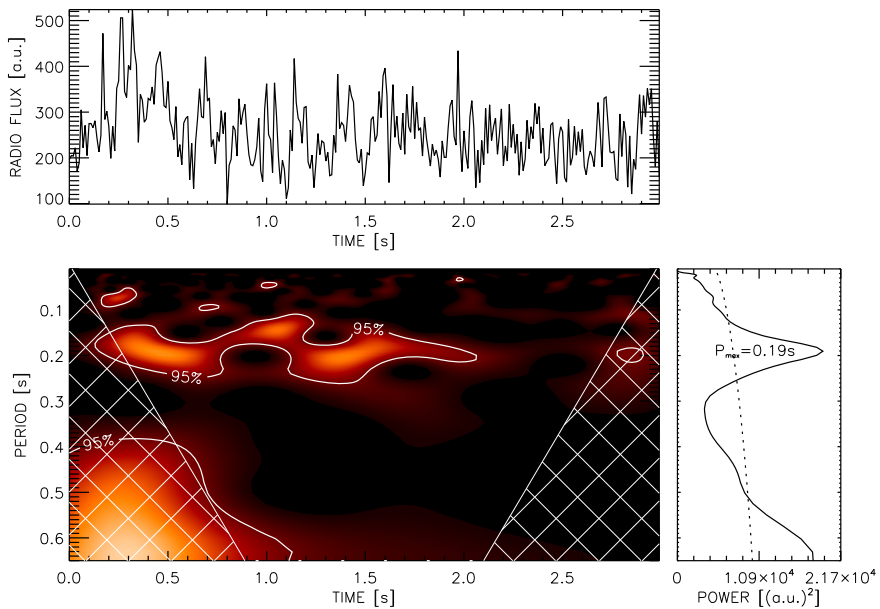


**Figure 6** The 1140 MHz radio flux, wavelet power spectrum, and integrated spectrum in the 13:42:00 – 13:42:03 UT interval of the 10 May 2022 event.

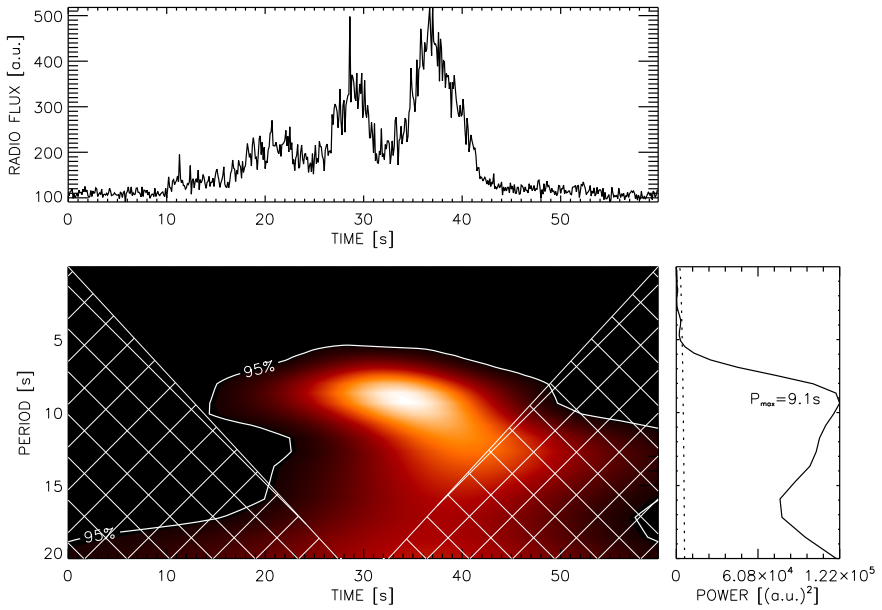


**Figure 7** The 1100 MHz radio flux, wavelet power spectrum and integrated spectrum in the 06:23:00–06:24:00 UT interval of the 26 August 2022 event.

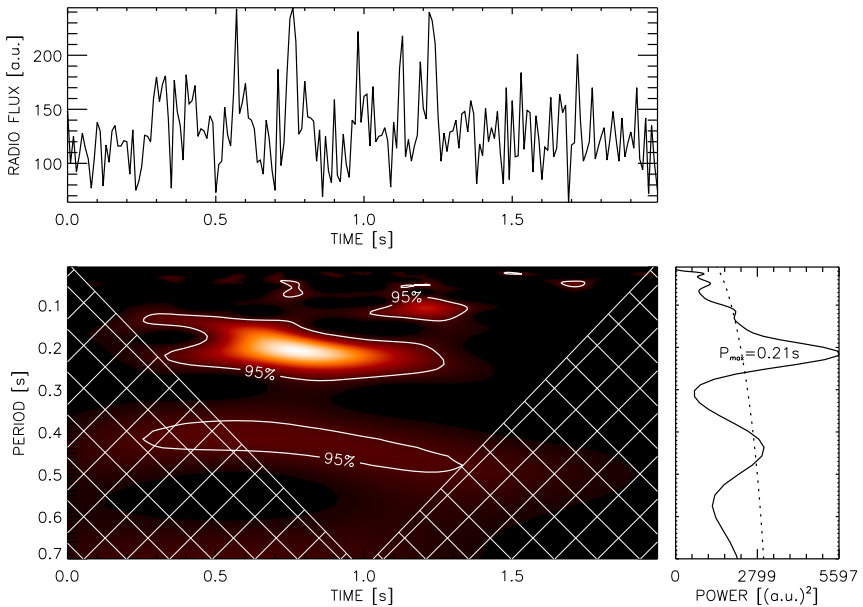


**Figure 8** The 1040 MHz radio flux, wavelet power spectrum and integrated spectrum in the 06:23:06–06:23:08 UT interval of the 26 August 2022 event.

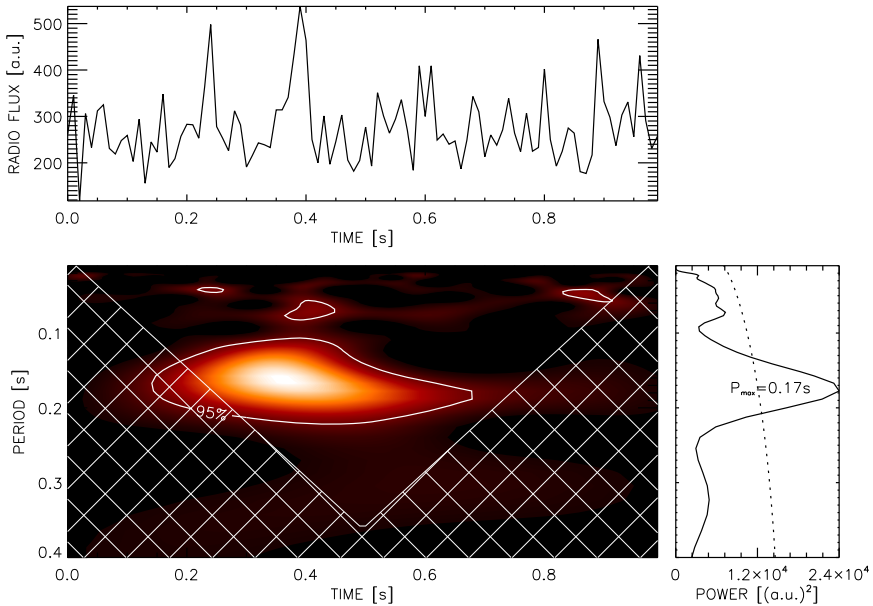


**Figure 9** The 1150 MHz radio flux, wavelet power spectrum, and integrated spectrum in the 06:23:27–06:23:28 UT interval of the 26 August 2022 event.

interval. Here the period is 0.17 s significant for the time interval 06:23:27.1–06:23:27.7 UT. All periods found for both flare events are summarized in Table 1.

### 3. EUV and X-ray Observations

The corresponding EUV flares are investigated using the imaging observations performed by the Atmospheric Imaging Assembly (AIA) onboard the Solar Dynamics Observatory (Lemen et al. 2012). AIA observes the full Sun and its corona up to about  $1.3 R_{\odot}$  in 10 EUV and UV channels, covering a wide range of plasma temperatures (see, for example, O’Dwyer et al. 2010; Del Zanna 2013). Here we primarily use the 94 Å channel for observations of hot flare plasma (dominated by Fe XVIII,  $\approx 8$  MK). During strong flares, this channel is not as saturated as the hotter 131 Å channel (Fe XXI,  $\approx 10$  MK). For the neighboring corona, we primarily use the 171 Å channel (Fe IX, formed below  $\approx 1$  MK), although the hotter channels of 193 Å (Fe XII,  $\approx 1.5$  MK) and 211 Å (Fe XIV,  $\approx 2$  MK) are reviewed as well. For the transition region plasmas, we use the 304 Å channel (He II,  $\leq 0.1$  MK). The 304 Å channel has degraded significantly in the past decade (Dos Santos et al. 2021); nevertheless, the useful signal can still be obtained, especially in bright areas, albeit at much lower counts. Animations of the AIA EUV observations were prepared and are available as the accompanying material.

Evolution of soft X-ray (SXR) flux during both flares was obtained by X-ray Sensor (XRS) onboard the Geostationary Operational Environmental Satellite (GOES). XRS provides solar X-ray irradiances for two wavelength bands, 0.5–4.0 Å and 1–8 Å. Finally, the measurements of the longitudinal component of the photospheric magnetic fields have been taken by the Helioseismic and Magnetic Imager (HMI, Scherrer et al. 2012).



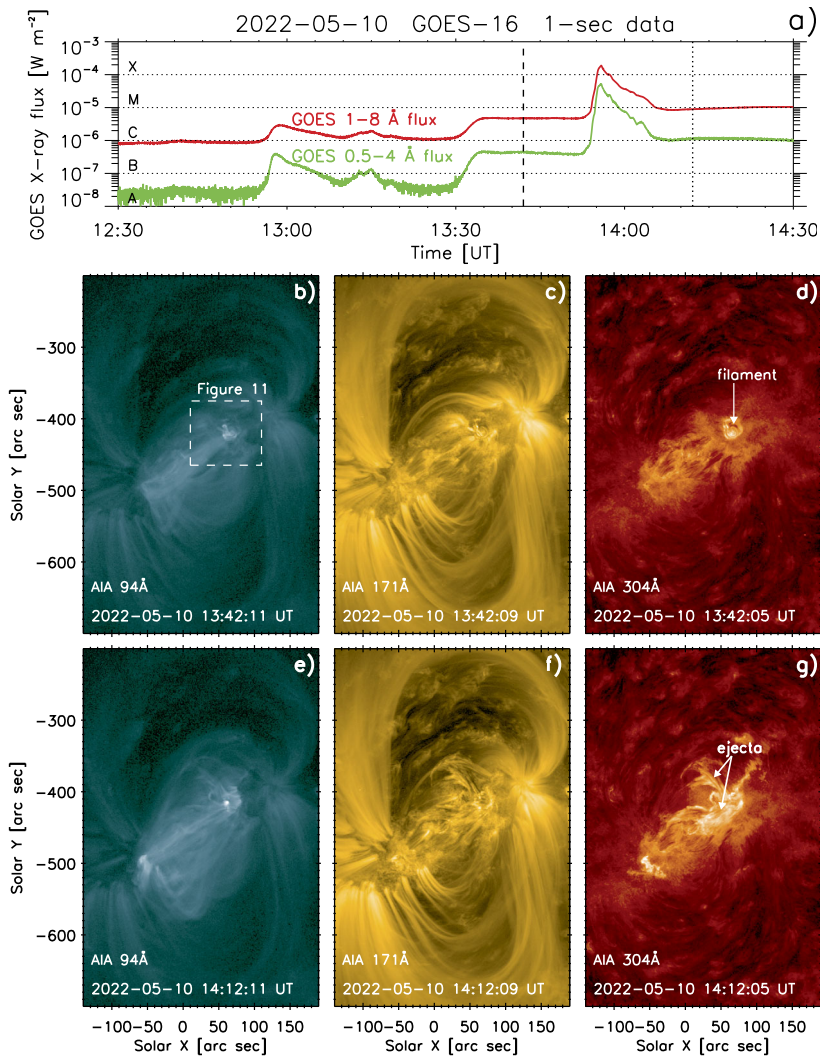


**Figure 10** Overview of the X1.5 X-ray flare and the flaring AR 13006 as observed by GOES-16 (a) and SDO/AIA (b)–(g). Three wavelengths are shown, 94 Å, 171 Å, and 304 Å. The dashed box indicates the field of view of Figure 11, and the vertical lines in panel (a) indicate the time of the AIA images shown. The thick dashed line corresponds to 13:42 UT, i.e., the time of the dm-spikes, as well as the time shown in panels (b)–(d). The 304 Å observations in panel (d) show a small filament, which produces bright ejecta visible after the X-ray flare in panel (g).

### 3.1. Event 1 – X1.5 Flare on 10 May 2022

The dm-spikes at 13:42 UT on 10 May 2022 occurred during the precursor phase of the X1.5-class X-ray flare as recorded by GOES-16 (see panel (a) of Figure 10). The flare itself had a short impulsive phase, whereas the gradual phase lasted only about 20 min. EUV observations show that the flare occurred in a highly localized circular region within the AR 13006, whose Hale class was  $\beta\delta/\beta$  (see Figures 10–11). Figure 10 shows the EUV

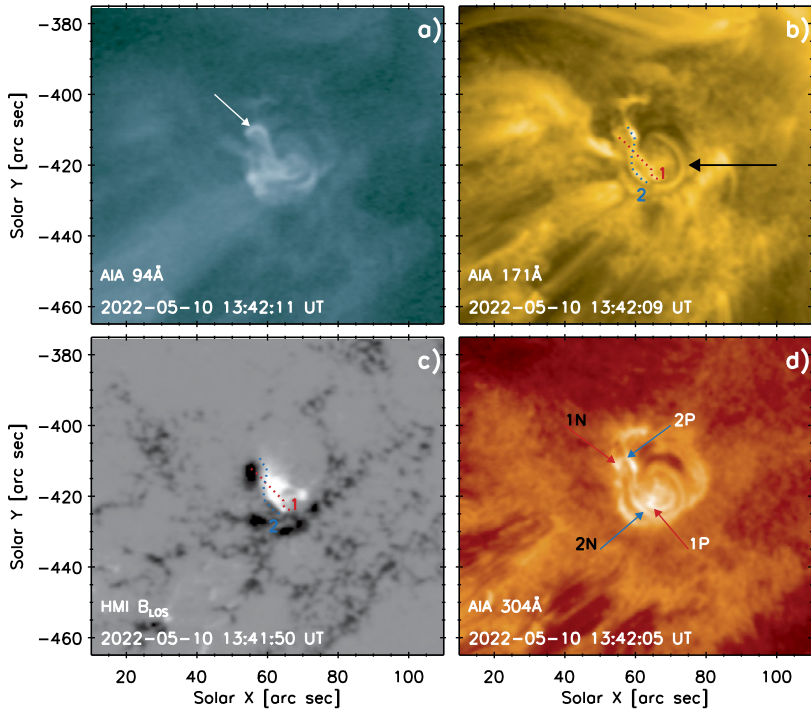


**Figure 11** Multiwavelength observations of reconnecting threads at the time of dm-spikes at about 13:42:09 UT. The reconnecting threads 1 (red) and 2 (blue) are both bright in 171 Å (b). The HMI magnetogram (c) shows these threads are oppositely oriented. Four bright kernels in 304 Å at their footpoints, denoted 1P/1N and 2P/2N, are shown in panel (d). A hot loop in AIA 94 Å connecting 1N and 2P is pointed out by a white arrow in panel (a).

observations of the AR 13006 at the time of the dm-spikes shortly after 13:42 UT (panels b–d) and after the flare at 14:12 UT (panels e–g). It is seen that the flare is associated with the eruption of a small filament best seen in 304 Å at 13:42 UT (white arrow in panel d). The small filament is also identifiable in 171 Å (panel c). Before its eruption, this filament was located wholly within the circular structure (see also Figure 11). The corresponding post-eruption ejecta are depicted in panel (g) of Figure 10. We note that during the impulsive and peak phases of the X1.5 flare, many AIA channels are saturated. At 14:12 UT, the ejecta do not form a closed rising eruptive filament. Instead, the majority of the plasma within the ejecta shown in Figure 10 (panel g) is falling back to the Sun. It is difficult to ascertain whether this flare is confined or eruptive based on AIA observations alone; nevertheless, a weak partial halo CME was reported after the flare at 14:36 UT by the LASCO CDAW catalog.<sup>1</sup>

Due to the fast nature of the flare X-ray curve, the presence of a circular structure in EUV observations, as well as at least a partial disintegration of the filament during eruption, we classify this flare as a null-point flare with flux rope eruption (the literature on null-point flares is extensive; see, e.g., Masson et al. 2009; Sun et al. 2013; Zhang et al. 2016; Sun

<sup>1</sup>[https://cdaw.gsfc.nasa.gov/CME\\_list/UNIVERSAL\\_ver1/2022\\_05/univ2022\\_05.html](https://cdaw.gsfc.nasa.gov/CME_list/UNIVERSAL_ver1/2022_05/univ2022_05.html).

et al. 2016; Romano et al. 2017; Joshi et al. 2017; Chen et al. 2018; Prasad et al. 2020; Li, Priest, and Guo 2021; Liu et al. 2021; Cheng et al. 2023; Zhang 2024).

Since the circular structure only spans about  $20''$  (see Figure 11), i.e., a size only  $\approx 13$  times the AIA resolution (which is  $1.5''$ ; see Lemen et al. 2012), identification of individual reconnecting structures is a difficult task. Nevertheless, at 13:42:09 UT, during the occurrence of dm-spikes (Figure 1), two bright crossing threads are seen in AIA 171 Å, denoted as 1 and 2. The overall structure of these crossing threads resembles the Greek letter  $\chi$  (see panel (b) of Figure 11). Denoting the respective footpoints in positive/negative polarities as 1P/1N and 2P/2N, respectively, and comparing with the underlying polarities as observed in the HMI  $B_{\text{LOS}}$  magnetogram (panel (c) of Figure 11), it is found that threads 1 and 2 are oppositely oriented at the location of their crossing. Thread 1 crosses from the local polarity inversion line (PIL) and connects the positive polarity with the locally strongest negative polarity (see panel c), whereas thread 2 straddles the PIL along much of its length. Furthermore, in all of the respective footpoints locations, a brightening (bright kernel) is observed in AIA 304 Å (see panel (d) of Figure 11).

Thread 1 is already visible at 13:40 UT (see the accompanying animation), whereas thread 2 brightens only somewhat later, being well visible in 171 Å at 13:41:39 UT. It brightens together with another semicircular filament thread, denoted by black arrow in Figure 11b. Therefore we interpret the situation as reconnection of thread 2 of the erupting flux rope (small filament) with an overlying loop 1, which is oppositely oriented. Such a reconnection scenario is supported by the fact that the footpoints 1N and 2P are connected by a small loop, which is bright in hot AIA channels such as 94 Å (white arrow in panel a). The situation between the conjugate footpoints 1P and 2N is not resolved by AIA, as there are several overlying and overlapping hot loops.

### 3.2. Event 2 – C7.2 Flare on 26 August 2022

During Event 2, the dm-spikes occur during the impulsive phase of the respective C7.2 X-ray flare (see the dashed line and the GOES X-ray curve in Figure 12a). This event is also a filament eruption, occurring in the AR 13088 located close to the SW limb of the Sun (see Figure 12 and the accompanying animation). Many overlapping systems of bright loops are seen in both warm (171 Å) and hot (94 Å) channels of AIA, attesting to the rather complicated magnetic structure of this AR, along with at least three systems of bright flare loops in 94 Å (see panel h). Therefore it is nearly impossible to find a unique pair of reconnecting structures at the time of the dm-spikes ( $\approx 06:23$  UT; see Figures 3–4). Nevertheless, we identified some common characteristics with Event 1:

- Presence of an erupting filament with bright threads along it from the start of the eruption (Figure 12, panel e).
- Disintegration of the original filament during its eruption (no coherent, contiguous erupting filament can be identified in Figure 12, panels f–g).
- Presence of only faint ejecta high in the corona post-eruption (white arrows in Figure 12, panel i).

Therefore the dm-spikes in Event 2 could also be associated with reconnection involving the erupting filament and its magnetic flux rope.

## 4. Discussion

Since the reconnecting structures were identified only in Event 1, we interpret the periods found and drifts in groups of dm-spikes only for the 10 May 2022 flare. However, we think

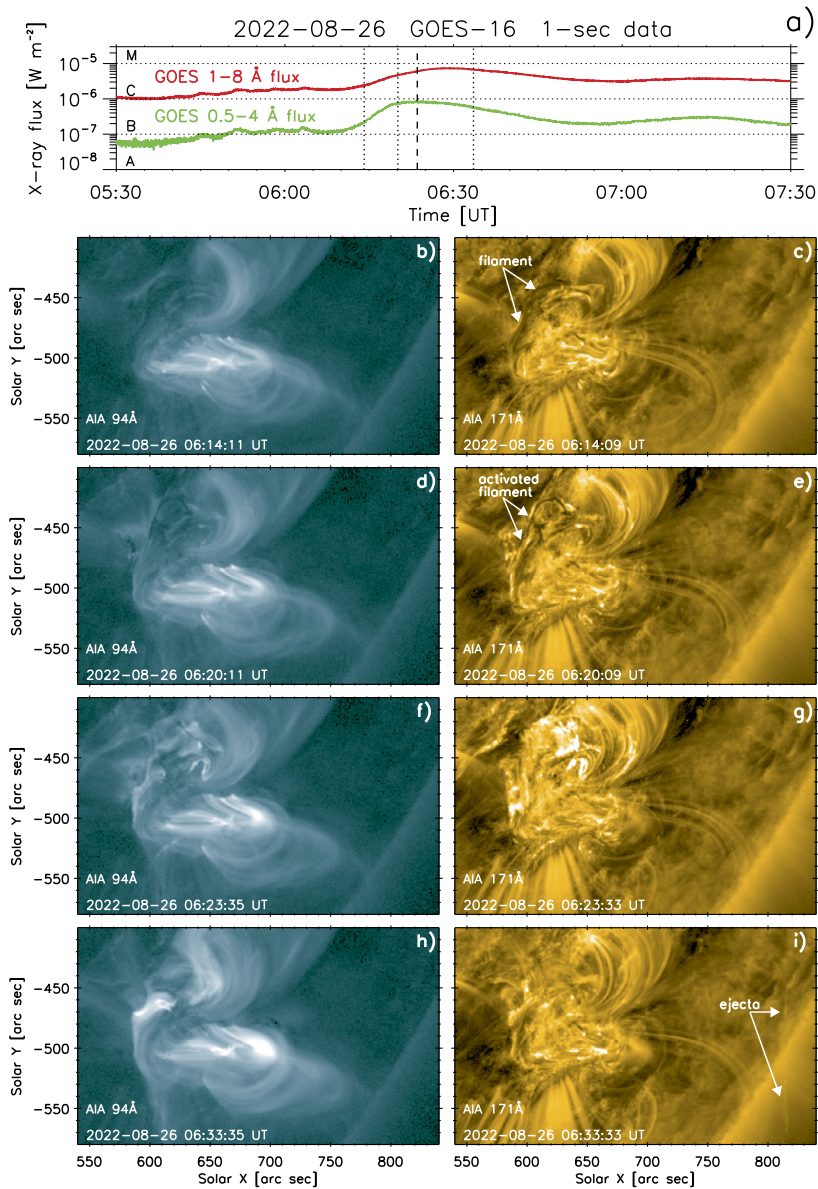


**Figure 12** Observations of the C7.2 X-ray flare and the flaring AR 13088 as observed on 26 August 2022 by GOES-16 (a) and SDO/AIA (b)–(i). The vertical lines in panel (a) indicate the times shown in panels (b)–(i). The thick dashed line corresponds to 06:23 UT and the dm-spikes in this Event 2. Many systems of hot and warm loops are seen in the AIA 94 Å (left) and 171 Å (right) observations, along with a filament that undergoes an eruption of which only faint ejecta (white arrows in panel (i)) survive.

that periods and drifts of spike groups in Event 2 are generated by similar processes as in Event 1.

SDO/AIA observations at the time of the spikes in Event 1 (Figure 11, panel b) show two loops mutually interacting, whose magnetic fields are oppositely oriented. Therefore there should be a current sheet formed between them, where the magnetic reconnection starts, electrons are accelerated, and the spikes are generated. Because groups of the spikes occurred quasi-periodically with the period  $\approx 5.1$  s, we propose that owing to a sudden start of the magnetic reconnection, one of the loops started to oscillate on the fundamental kink mode and thus quasi-periodically modulate the reconnection process.

Let us estimate the magnetic field in the oscillating loop. Assuming that the loop that is uniform and the mass density out of the loop is very low, the period of loop oscillation is (Nakariakov et al. 2021)

$$P_{\text{kink}} = \frac{2L}{C_{\text{kink}}}, \quad (1)$$

where  $L$  is the loop length, and  $C_{\text{kink}}$  is the kink speed equal to the Alfvén speed in the loop. Then from this relation we can express the magnetic field in the loop as

$$B = \frac{2L}{P_{\text{kink}}} \sqrt{4\pi\rho_i}, \quad (2)$$

where  $\rho_i = m_p n_e$  is the mass density,  $m_p$  is the proton mass, and  $n_e$  is the plasma density.

Assuming that spikes are generated on the frequency close to the plasma frequency and the corresponding plasma density is close to the density in the loop, the loop density is  $n_e \approx 1.5 \times 10^{10} \text{ cm}^{-3}$  for the mean spike frequency 1100 MHz. Now estimating the length of loop 1 as  $L \sim 15''$  and considering the oscillation period  $\sim 5.1$  s, the magnetic field in loop 1 is 240 G. Loop 2 is longer ( $L \approx 23''$ ). It gives the magnetic field in loop 2 as 370 G. We note that because of the above-mentioned assumptions, it is a rough estimation. For comparison, the magnetic field at the regions of loop footpoints is of the order of several hundred G.

Besides the main period 5.1 s, in Event 1, we found a much shorter period of 0.19 s. We propose that this short period could be caused by quasi-periodic particle acceleration episodes, which result from a dynamic phase of magnetic reconnection. The reconnection is dominated by the repeated formation and subsequent coalescence of magnetic islands, known as “secondary tearing” or “impulsive bursty” regime of reconnection (Kliem, Karlický, and Benz 2000).

During this reconnection, electrons are accelerated and propagate into the reconnecting plasma outflows and generate dm-spikes. This scenario agrees with the results of our previous studies that the dm-spikes are generated in the magnetohydrodynamic turbulence in the reconnecting plasma outflows (Karlický, Sobotka, and Jiříčka 1996; Karlický, Benáček, and Rybák 2021). Just these reconnection outflows can explain the frequency drift of the spike groups detected. Electrons accelerated in the magnetic reconnection and generating spikes are trapped in the plasma reconnection outflow, which moves to higher or lower plasma densities. Thus spike groups drift to higher or lower frequencies, assuming that the spikes are generated by the plasma emission mechanism.

Similar short periods in a similar frequency range were shown by Zhang et al. (2015) and Huang et al. (2022). Zhang et al. (2015) found the periods in the range 0.1–0.3 s in association with the filament motions, loop brightening in the EUV imaging observations, and nonthermal hard X-ray emission enhancements. Furthermore, Huang et al. (2022) have shown the synchronous quasi-periodic oscillations of spikes and pulsations with the periods 0.1–0.9 s. They explained these oscillations by the quasi-periodic acceleration of electrons due to the tearing-mode oscillations, which is the same process as proposed in our case.

Namely, the tearing instability forms plasmoids. The only difference is that whereas they consider these quasi-periodic accelerations in a confined flux rope, we propose these accelerations in the current sheet.

## 5. Conclusions

In two flares on 10 May 2022 and 26 August 2022, we presented and analyzed groups of the dm-spikes that occurred quasi-periodically. Besides their global periods (5.1 s for the 10 May 2022 flare and 9.1 s for the 26 August 2022 one), we found subgroups of spikes having the periods 0.19 s in the 10 May 2022 flare and 0.17 s and 0.21 s in the 26 August 2022 flare. Some of these subgroups of spikes even drifted with a positive (930, 1100, and 1710 MHz s<sup>-1</sup>) or negative (-1000 and -1330 MHz s<sup>-1</sup>) frequency drift.

During the 10 May 2022 flare, at the time of the dm-spikes, the SDO/AIA 171 Å images showed the region where two bright short loops with oppositely oriented magnetic fields interacted. One of these loops was interpreted as a bright thread belonging to the small erupting filament, whereas the other loop was likely an overlying one. Based on these observations, we propose that the dm-spikes were generated during the magnetic reconnection of these loops. The magnetic reconnection was not only in the dynamic quasi-periodic regime and caused the period 0.19 s, but this reconnection was also modulated by an oscillation of one of the interacting loops and thus caused the period 5.1 s. During this process, accelerated electrons were trapped in reconnecting plasma outflows, and thus the drifting groups of spikes were generated.

The 26 August 2022 flare was accompanied by a filament eruption and contained several systems of flare loops, making the identification of the individual reconnecting structures difficult. However, this event shared some common characteristics with the 10 May 2022 event, namely, the presence of an erupting filament accompanied by bright threads and ultimate disintegration of the filament during the course of its eruption. This means that the periods and drifts of the spike groups in the 26 August 2022 event were likely generated by a similar process as in the 10 May 2022 flare.

**Supplementary Information** The online version contains supplementary material available at <https://doi.org/10.1007/s11207-024-02359-y>.

**Acknowledgments** AIA and HMI data are courtesy of NASA/SDO and the AIA and HMI science teams.

**Author contributions** MK: radio data selection, interpretation JD: AIA/SDO data analysis JR: wavelet analysis of radio data All authors reviewed the manuscript.

**Funding** Open access funding provided by The Ministry of Education, Science, Research and Sport of the Slovak Republic in cooperation with Centre for Scientific and Technical Information of the Slovak Republic. M.K. and J.D. acknowledge institutional support from the project RVO-67985815. M.K. also acknowledges support from the GA ČR grant 22-34841S. J.R. acknowledges support from the Science Grant Agency project VEGA 2/0043/24 (Slovakia).

**Data Availability** No datasets were generated or analysed during the current study.

## Declarations

**Competing interests** The authors declare no competing interests.

**Open Access** This article is licensed under a Creative Commons Attribution 4.0 International License, which permits use, sharing, adaptation, distribution and reproduction in any medium or format, as long as you give appropriate credit to the original author(s) and the source, provide a link to the Creative Commons licence, and indicate if changes were made. The images or other third party material in this article are included in the article's Creative Commons licence, unless indicated otherwise in a credit line to the material. If material is not included in the article's Creative Commons licence and your intended use is not permitted by statutory regulation or exceeds the permitted use, you will need to obtain permission directly from the copyright holder. To view a copy of this licence, visit <http://creativecommons.org/licenses/by/4.0/>.

## References

- Aschwanden, M.J., Dennis, B.R., Benz, A.O.: 1998, Logistic avalanche processes, elementary time structures, and frequency distributions in solar flares. *Astrophys. J.* **497**, 972. [DOI](#). [ADS](#).
- Bárta, M., Karlický, M.: 2001, Turbulent plasma model of the narrowband dm-spikes. *Astron. Astrophys.* **379**, 1045. [DOI](#). [ADS](#).
- Benz, A.O.: 1986, Millisecond radio spikes. *Solar Phys.* **104**, 99. [DOI](#). [ADS](#).
- Bouratzis, C., Hillaris, A., Alissandrakis, C.E., Preka-Papadema, P., Moussas, X., Caroubalos, C., Tsitsipis, P., Kontogeorgos, A.: 2016, High resolution observations with artemis-IV and the NRH. I. Type IV associated narrow-band bursts. *Astron. Astrophys.* **586**, A29. [DOI](#). [ADS](#).
- Chen, B., Yu, S., Battaglia, M., Farid, S., Savcheva, A., Reeves, K.K., Krucker, S., Bastian, T.S., Guo, F., Tassev, S.: 2018, Magnetic reconnection null points as the origin of semirelativistic electron beams in a solar jet. *Astrophys. J.* **866**, 62. [DOI](#). [ADS](#).
- Cheng, X., Priest, E.R., Li, H.T., Chen, J., Aulanier, G., Chitta, L.P., Wang, Y.L., Peter, H., Zhu, X.S., Xing, C., Ding, M.D., Solanki, S.K., Berghmans, D., Teriaca, L., Aznar Cuadrado, R., Zhukov, A.N., Guo, Y., Long, D., Harra, L., Smith, P.J., Rodriguez, L., Verbeeck, C., Barczynski, K., Parenti, S.: 2023, Ultra-high-resolution observations of persistent null-point reconnection in the solar corona. *Nat. Commun.* **14**, 2107. [DOI](#). [ADS](#).
- Del Zanna, G.: 2013, The multi-thermal emission in solar active regions. *Astron. Astrophys.* **558**, A73. [DOI](#). [ADS](#).
- Dos Santos, L.F.G., Bose, S., Salvatelli, V., Neuberg, B., Cheung, M.C.M., Janvier, M., Jin, M., Gal, Y., Boerner, P., Baydin, A.G.: 2021, Multichannel autocalibration for the atmospheric imaging assembly using machine learning. *Astron. Astrophys.* **648**, A53. [DOI](#). [ADS](#).
- Droege, F.: 1977, Millisecond fine-structures of solar burst radiation in the range 0.2–1.4 GHz. *Astron. Astrophys.* **57**, 285. [ADS](#).
- Fleishman, G.D., Gary, D.E., Nita, G.M.: 2003, Decimetric spike bursts versus microwave continuum. *Astrophys. J.* **593**, 571. [DOI](#). [ADS](#).
- Fleishman, G.D., Mel'nikov, V.F.: 1998, REVIEWS OF TOPICAL PROBLEMS: millisecond solar radio spikes. *Phys. Usp.* **41**, 1157. [DOI](#). [ADS](#).
- Guedel, M.: 1990, Solar radio spikes - radiation at harmonics  $S = 2-6$ . *Astron. Astrophys.* **239**, L1. [ADS](#).
- Huang, J., Tan, C., Chen, X., Tan, B., Yan, Y., Zhang, Y., Ma, S., Zhou, Z., Zhang, M., Wang, W., Chen, L.: 2022, Clusters of solar radio spikes modulated by quasi-periodic pulsations in a confined flare. *Universe* **8**, 348. [DOI](#). [ADS](#).
- Jiříčka, K., Karlický, M.: 2008, Narrowband pulsating decimeter structure observed by the new Ondřejov solar radio spectrograph. *Solar Phys.* **253**, 95. [DOI](#). [ADS](#).
- Joshi, N.C., Sterling, A.C., Moore, R.L., Magara, T., Moon, Y.-J.: 2017, Onset of a large ejective solar eruption from a typical coronal-jet-base field configuration. *Astrophys. J.* **845**, 26. [DOI](#). [ADS](#).
- Karlický, M., Benáček, J., Rybák, J.: 2021, Narrowband spikes observed during the 2013 November 7 flare. *Astrophys. J.* **910**, 108. [DOI](#). [ADS](#).
- Karlický, M., Sobotka, M., Jiříčka, K.: 1996, Narrowband dm-spikes in the 2 GHz frequency range and MHD cascading waves in reconnection outflows. *Solar Phys.* **168**, 375. [DOI](#). [ADS](#).
- Karlický, M., Rybák, J., Benáček, J., Kašparová, J.: 2022, Narrowband spikes observed during the 13 June 2012 flare in the 800–2000 MHz range. *Solar Phys.* **297**, 54. [DOI](#). [ADS](#).
- Kliem, B., Karlický, M., Benz, A.O.: 2000, Solar flare radio pulsations as a signature of dynamic magnetic reconnection. *Astron. Astrophys.* **360**, 715. [arXiv](#). [ADS](#).
- Krucker, S., Benz, A.O.: 1994, The frequency ratio of bands of microwave spikes during solar flares. *Astron. Astrophys.* **285**, 1038. [ADS](#).
- Lemen, J.R., Title, A.M., Akin, D.J., Boerner, P.F., Chou, C., Drake, J.F., Duncan, D.W., Edwards, C.G., Friedlaender, F.M., Heyman, G.F., Hurlburt, N.E., Katz, N.L., Kushner, G.D., Levay, M., Lindgren, R.W., Mathur, D.P., McFeaters, E.L., Mitchell, S., Rehse, R.A., Schrijver, C.J., Springer, L.A., Stern,

- R.A., Tarbell, T.D., Wuelser, J.-P., Wolfson, C.J., Yanari, C., Bookbinder, J.A., Cheimets, P.N., Caldwell, D., Deluca, E.E., Gates, R., Golub, L., Park, S., Podgorski, W.A., Bush, R.I., Scherrer, P.H., Gumm, M.A., Smith, P., Auker, G., Jerram, P., Pool, P., Soufli, R., Windt, D.L., Beardsley, S., Clapp, M., Lang, J., Waltham, N.: 2012, The Atmospheric Imaging Assembly (AIA) on the Solar Dynamics Observatory (SDO). *Solar Phys.* **275**, 17. DOI. ADS.
- Li, T., Priest, E., Guo, R.: 2021, Three-dimensional magnetic reconnection in astrophysical plasmas. *Proc. Roy. Soc. London Ser. A* **477**, 20200949. DOI. ADS.
- Liu, L., Liu, J., Chen, J., Wang, Y., Wang, G., Zhou, Z., Cui, J.: 2021, The configuration and failed eruption of a complex magnetic flux rope above a  $\delta$  sunspot region. *Astron. Astrophys.* **648**, A106. DOI. ADS.
- Masson, S., Pariat, E., Aulanier, G., Schrijver, C.J.: 2009, The nature of flare ribbons in coronal null-point topology. *Astrophys. J.* **700**, 559. DOI. ADS.
- Melrose, D.B.: 2017, Coherent emission mechanisms in astrophysical plasmas. *Rev. Mod. Plasma Phys.* **1**, 5. DOI. ADS.
- Melrose, D.B., Dulk, G.A.: 1982, Electron-cyclotron masers as the source of certain solar and stellar radio bursts. *Astrophys. J.* **259**, 844. DOI. ADS.
- Messmer, P., Benz, A.O.: 2000, The minimum bandwidth of narrowband spikes in solar flare decimetric radio waves. *Astron. Astrophys.* **354**, 287. ADS.
- Nakariakov, V.M., Anfinogentov, S.A., Antolin, P., Jain, R., Kolotkov, D.Y., Kupriyanova, E.G., Li, D., Magyar, N., Nistić, G., Pascoe, D.J., Srivastava, A.K., Terradas, J., Vashghani Farahani, S., Verth, G., Yuan, D., Zimovets, I.V.: 2021, Kink oscillations of coronal loops. *Space Sci. Rev.* **217**, 73. DOI. ADS.
- Nita, G.M., Fleishman, G.D., Gary, D.E., Marin, W., Boone, K.: 2014, Fitting FFT-derived spectra: theory, tool, and application to solar radio spike decomposition. *Astrophys. J.* **789**, 152. DOI. ADS.
- O'Dwyer, B., Del Zanna, G., Mason, H.E., Weber, M.A., Tripathi, D.: 2010, SDO/AIA response to coronal hole, quiet Sun, active region, and flare plasma. *Astron. Astrophys.* **521**, A21. DOI. ADS.
- Prasad, A., Dissauer, K., Hu, Q., Bhattacharyya, R., Veronig, A.M., Kumar, S., Joshi, B.: 2020, Magneto-hydrodynamic simulation of magnetic null-point reconnections and coronal dimmings during the X2.1 flare in NOAA AR 11283. *Astrophys. J.* **903**, 129. DOI. ADS.
- Romano, P., Falco, M., Guglielmino, S.L., Murabito, M.: 2017, Observation of a 3D magnetic null point. *Astrophys. J.* **837**, 173. DOI. ADS.
- Rozhansky, I.V., Fleishman, G.D., Huang, G.-L.: 2008, Millisecond microwave spikes: statistical study and application for plasma diagnostics. *Astrophys. J.* **681**, 1688. DOI. ADS.
- Scherrer, P.H., Schou, J., Bush, R.I., Kosovichev, A.G., Bogart, R.S., Hoeksema, J.T., Liu, Y., Duvall, T.L., Zhao, J., Title, A.M., Schrijver, C.J., Tarbell, T.D., Tomczyk, S.: 2012, The Helioseismic and Magnetic Imager (HMI) investigation for the Solar Dynamics Observatory (SDO). *Solar Phys.* **275**, 207. DOI. ADS.
- Staelhi, M., Magun, A.: 1986, The microwave spectrum of solar millisecond spikes. *Solar Phys.* **104**, 117. DOI. ADS.
- Stepanov, A.V., Kliem, B., Krüger, A., Hildebrandt, J., Garaimov, V.I.: 1999, Second-harmonic plasma radiation of magnetically trapped electrons in stellar coronae. *Astrophys. J.* **524**, 961. DOI. ADS.
- Sun, X., Hoeksema, J.T., Liu, Y., Aulanier, G., Su, Y., Hannah, I.G., Hock, R.A.: 2013, Hot spine loops and the nature of a late-phase solar flare. *Astrophys. J.* **778**, 139. DOI. ADS.
- Sun, J.Q., Zhang, J., Yang, K., Cheng, X., Ding, M.D.: 2016, Observation of magnetic reconnection at a 3D null point associated with a solar eruption. *Astrophys. J. Lett.* **830**, L4. DOI. ADS.
- Tan, B.: 2013, Small scale microwave bursts in long-duration solar flares. *Astrophys. J.* **773**, 165. DOI. ADS.
- Tan, C., Yan, Y., Tan, B., Fu, Q., Liu, Y., Xu, G.: 2015, Study of calibration of solar radio spectrometers and the quiet-sun radio emission. *Astrophys. J.* **808**, 61. DOI. ADS.
- Torrence, C., Compo, G.P.: 1998, A Practical Guide to Wavelet Analysis. *Bulletin of the American Meteorological Society*, 61–71. DOI. ADS.
- Willes, A.J., Robinson, P.A.: 1996, Electron-cyclotron maser theory for noninteger ratio emission frequencies in solar microwave spike bursts. *Astrophys. J.* **467**, 465. DOI. ADS.
- Winglee, R.M., Dulk, G.A., Pritchett, P.L.: 1988, Fine structure of microwave spike bursts and associated cross-field energy transport. *Astrophys. J.* **328**, 809. DOI. ADS.
- Zhang, Q.: 2024, Circular-ribbon flares and the related activities. *Rev. Mod. Plasma Phys.* **8**, 7. DOI. ADS.
- Zhang, Y., Tan, B., Karlický, M., Mészárosová, H., Huang, J., Tan, C., Simões, P.J.A.: 2015, Solar radio bursts with spectral fine structures in preflares. *Astrophys. J.* **799**, 30. DOI. ADS.
- Zhang, Q.M., Li, D., Ning, Z.J., Su, Y.N., Ji, H.S., Guo, Y.: 2016, Explosive chromospheric evaporation in a circular-ribbon flare. *Astrophys. J.* **827**, 27. DOI. ADS.